Simulated and Experimental Damping Properties of a SMA/Fiber Glass Laminated Composite

S. Arnaboldi, P. Bassani, C.A. Biffi, A. Tuissi, M. Carnevale, N. Lecis, A. LoConte, and B. Previtali

(Submitted June 17, 2010; in revised form February 9, 2011)

In this article, an advanced laminated composite is developed, combining the high damping properties of shape memory alloy (SMA) with mechanical properties and light weight of a glass-fiber reinforced polymer. The composite is formed by stacking a glass-fiber reinforced epoxy core between two thin patterned strips of SMA alloy, and two further layers of fiber-glass reinforced epoxy. The bars of the laminated composite were assembled and cured in autoclave. The patterning was designed to enhance the interface adhesion between matrix and SMA inserts and optimally exploit the damping capacity of the SMA thin ribbons. The patterned ribbons of the SMA alloy were cut by means of a pulsed fiber laser source. Damping properties at different amplitudes on full scale samples were investigated at room temperature with a universal testing machine through dynamic tension tests, while temperature dependence was investigated by dynamic mechanical analyses (DMA) on smaller samples. Experimental results were used in conjunction with FEM analysis to optimize the geometry of the inserts. Experimental decay tests on the laminated composite have been carried out to identify the adimensional damping value related to their first flexural mode.

1. Introduction

Shape memory alloys (SMAs) are characterized by the well-known shape memory effect and pseudo-elasticity (Ref 1) as well as by a significant damping capacity. Combining these important functional properties of SMAs with the mechanical properties of glass-fiber reinforced polymers (GFRPs), smart and light-weight composite materials can be created, suitable to many structural applications where vibrational control is a critical design parameter (Ref 2). To enhance the damping capacity of a GFRP beam through passive vibration suppression, a SMA can be either bonded onto the beam or integrated into it. SMA shapes as fibers, ribbons, and films have been the object of many researches and development projects and the improved damping performance associated to SMA intrinsic properties was demonstrated (Ref 3). Textile composites obtained with SMA wires have also been investigated with promising results (Ref 4).

In this research study, due to the well-known difficulties in machining NiTi SMA alloys by traditional chip removal

processes (Ref 5), laser technology was selected to cut NiTiCu patterned ribbons for the production of discontinuous SMA composite materials. In literature, a great number of works was published on laser cutting and microcutting processes of NiTi alloys, mainly for stent applications in biomedical field (Ref 6, 7). Microgripper systems and microactuators for sensor and position control applications were also developed (Ref 8). However, to the authors' knowledge, issues about composite manufacturing, as related to SMA insert shape optimization and technology of insert cutting, were not deeply investigated.

In this article, an advanced laminated composite, characterized by a glass-fiber reinforced epoxy core embedded into two thin patterned ribbons of SMA material and two further layers of glass-fiber reinforced epoxy, is developed. The patterning of the SMA is optimized to enhance the adherence of the interface between composite matrix (the epoxy resin) and the insert itself. Damping properties of the SMA material were experimentally investigated, at room temperature and at different amplitudes, through dynamic tension tests on the SMA thin sheets. Temperature dependence of the SMA damping capacity was studied with dynamic mechanical analysis (DMA) on smaller samples. The obtained results were used in conjunction with FEM analysis to optimize the patterning geometry of the SMA inserts of the composite.

Prototype of the optimized composite has been manufactured and experimental decay tests on the produced laminated composites have been carried out to identify the adimensional damping value related to their first flexural mode.

2. Experimental

2.1 Thin SMA Ribbon Production

High-purity Ni, Ti and Cu metals were melted by means of a vacuum induction melting furnace (Balzers VSG 10) in an

S. Arnaboldi, P. Bassani, C.A. Biffi, and **A. Tuissi,** CNR Institute for Energetics and Interphases, Corso Promessi Sposi, 29, Lecco, Italy; and **M. Carnevale, N. Lecis, A. LoConte,** and **B. Previtali,** Department of Mechanical Engineering, Politecnico di Milano, Via La Masa, 34, Milan, Italy. Contact e-mail: paola.bassani@ieni.cnr.it.

isostatic graphite crucible. The nominal atomic composition of the produced SMA is $Ni_{40}Ti_{50}Cu_{10}$. The ingot, after hot forging and rolling at 950 °C, was cold straight rolled down to 0.2 mm thick and 30 mm width tapes. For this work strips of 200 mm in length were cut from cold rolled tapes, heat treated at 400 °C for 1 and then water quenched (WQ). Details about the SMA ribbon manufacturing were already published elsewhere (Ref. 9).

Calorimetric analyses of specimens, taken from the heat-treated ribbons, were performed with a DSC TA Q100, calibrated with a standard indium reference. The NiTiCu samples for DSC weighted about 6 mg and the heating/cooling rate was of 10 °C/min. A typical DSC scan of the produced strips after heat treatment and WQ is shown in Fig. 1.

2.2 Design of the Patterning of SMA Ribbon

The geometry of the patterning as well as the thickness of the SMA ribbons were optimized by FEM. Models with brick elements simulating the elastic material behavior were used and two different patterning geometries characterized by elliptical features were selected. The selected patterns allow optimally exploiting the damping capacity of the SMA ribbons and, in particular, enhancing the interface adhesion between matrix and SMA inserts. Improved interface strength would locally increase the SMA strain amplitude and hence the vibrational energy transmitted to the SMA inserts.

Table 1 lists the geometrical features of the SMA inserts.

In the SMA ribbon design, the problem related to the width of the ribbon edges (where the elliptical features are not present), was also taken into account. Figure 2 shows the stress distribution for the large ellipse ribbon. The simulation clearly
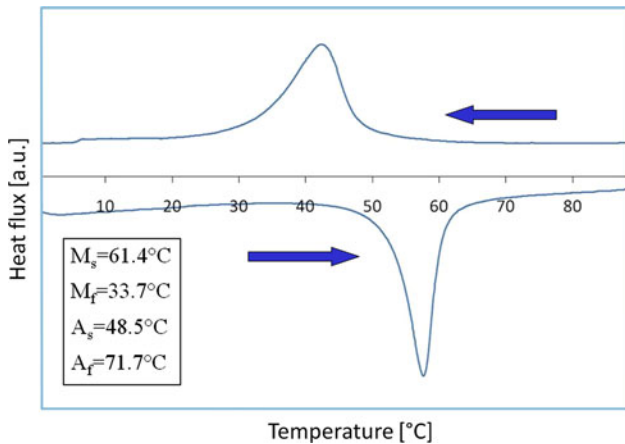

Fig. 1 DSC scan and phase-transformation temperatures of $Ni_{40}Ti_{50}Cu_{10}$ strip

Table 1   Main geometrical parameters of the two elliptical patterns

	Major semiaxis, mm	Minor semiaxis, mm	Major semiaxis / Minor semiaxis	Hole surface / Total surface
Large ellipse	4.5	2.25	2	2.40
Small ellipse	1.5	1	1.5	1.32

shows that larger edge (1 mm of pattern-free material at the edges of the strip) leads to a higher local stress than the 0.5 mm pattern-free edge. A similar behavior was also found for the small-ellipse strip design.

2.3 Laser Microcutting of the SMA Ribbon

A YLP-50 pulsed fiber laser source from IPG Photonics was used to perform the ribbon patterning. In Fig. 3(a), the laser system equipped with a LaserMech cutting head for microma-chining is shown. Figure 3(b) shows samples of the machined patterns (large and small ellipses) on the NiTiCu ribbons. The process parameters were optimized to guarantee the machining of a stable through cutting edge, high productivity (high process speed) and minimal amount of spatter and melted material, which are of great importance in nanosecond laser processing due to the relevant heat conduction inside the workpiece (Ref 10).

Argon flow at a pressure of 5 bar was used as inert gas shielding to cover the working area and to remove the melted material. Two laser passes at 50 mm/s process speed were adopted to perform the NiTiCu patterning. The maximum available power (50 W) and the maximum pulse frequency (80 kHz) were selected. The focus of the laser beam was fixed on the top surface of the NiTiCu ribbons to reach the minimum laser spot diameter, which was calculated to be about 23 μm in this configuration.

2.4 Laminated Composite Production

The last step of the production process is related to the production of the composite. In particular, glass-fiber reinforced epoxy core is covered by the two patterned NiTiCu ribbons that were in turn externally covered by an outer layer of glass-fiber reinforced epoxy. The scheme of the proposed laminated composite is shown in Fig. 4(a).

In order to characterize the dynamic properties of the designed laminated composite and to evaluate the improvement of the damping capacity due to the introduction of the SMA inserts, four samples of the composite, having thickness of 5 mm, width of 25 mm, and length of 200 mm were produced. The first sample was a glass-fiber reinforced epoxy beam with regular and symmetric angle-ply lamination, made with SP250 S29A Unidirectional S2 Glass/125 °C curing epoxy resin manufactured by 3 M. The sequence of lamination was $[45/-45]_{11}$. In the second sample, two SMA thin ribbons were embedded, respectively, below the upper and the lower surface of the beam. In the third and fourth beams, the inserted SMA thin ribbons were laser patterned in the large and small elliptical configurations. The number of fiber glass slides in the last three composite samples (with SMA inserts) were calculated to obtain the same thickness of the first composite sample (characterized by only fiber glass). The bars of the laminated composite were assembled and cured in autoclave. The four produced samples are shown in Fig. 4(b).

3. Results

3.1 Characterization of SMA Laser Patterned Ribbon Performances

Damping properties at different amplitudes and at a fixed frequency (0.05 Hz) on full-scale sample (20 × 200 mm) were
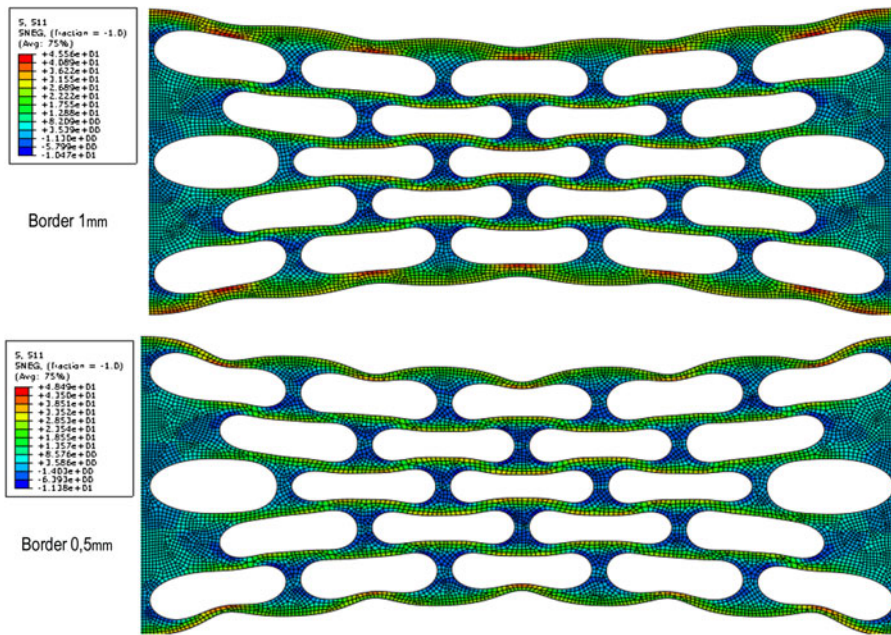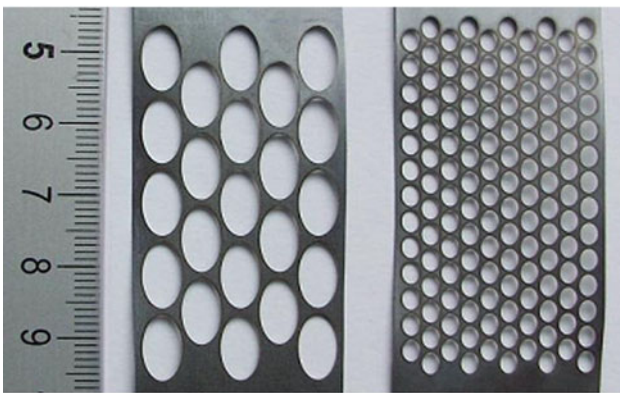
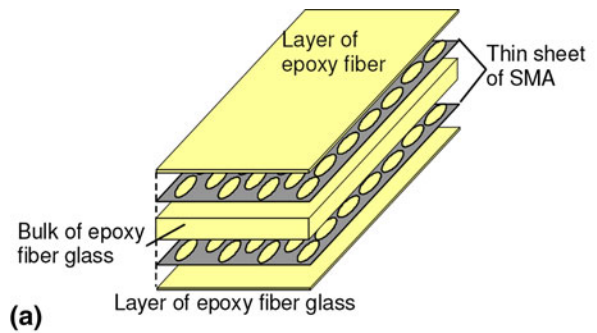**Fig. 2** Effect of the no-patterned edge size in the case of large ellipses in the simulation of tensile testing
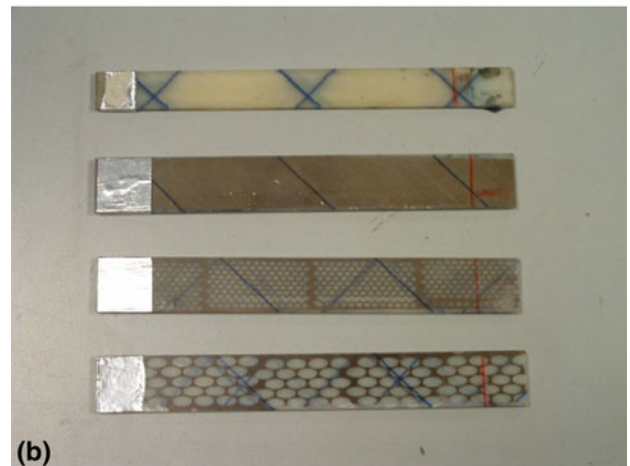

Fig. 3 Laser system adopted for NiTiCu microcutting (a) and patterned (b) NiTiCu ribbons in the two elliptical configurations

Fig. 4 Scheme of the SMA/fiber glass laminated composite (a) and the produced composite (b)

investigated at room temperature with an MTS testing frame through dynamic tension tests. Besides, temperature dependence on damping properties was investigated using TA Q800 dynamic mechanical analyzer (DMA) on smaller samples

selecting heating and cooling rates of 1 °C/min at 10 Hz and with 0.05% strain amplitude. All obtained data were introduced in the FEM simulation to predict the behavior of the laminated composites. In order to characterize damping properties, tan δ was used as a damping parameter:

$$\tan \delta = E_i/E_s, \qquad \text{(Eq 1)}$$

where E_i is the imaginary part of the complex modulus of the SMA and E_s is the storage modulus. Similarly, the h parameter was used as a further damping indicator:

$$h = r/2m\,\omega_0 = \tan \delta/2, \qquad \text{(Eq 2)}$$

where r is the viscous damping coefficient and $2\,m\,\omega_0$ represents the critical damping. The relationship between tan δ and h is reported in Eq (2).

In Fig. 5(a), the tensile test configuration is depicted. A 50 mm gage length extensometer was adopted for the tests. In Fig. 5(b), main results in terms of damping properties of NiTiCu ribbons in both patterned and not patterned conditions are reported. From statistical analysis of damping results, it can be stated that the ribbon condition (not patterned or patterned with small and large ellipses) does not affect significantly
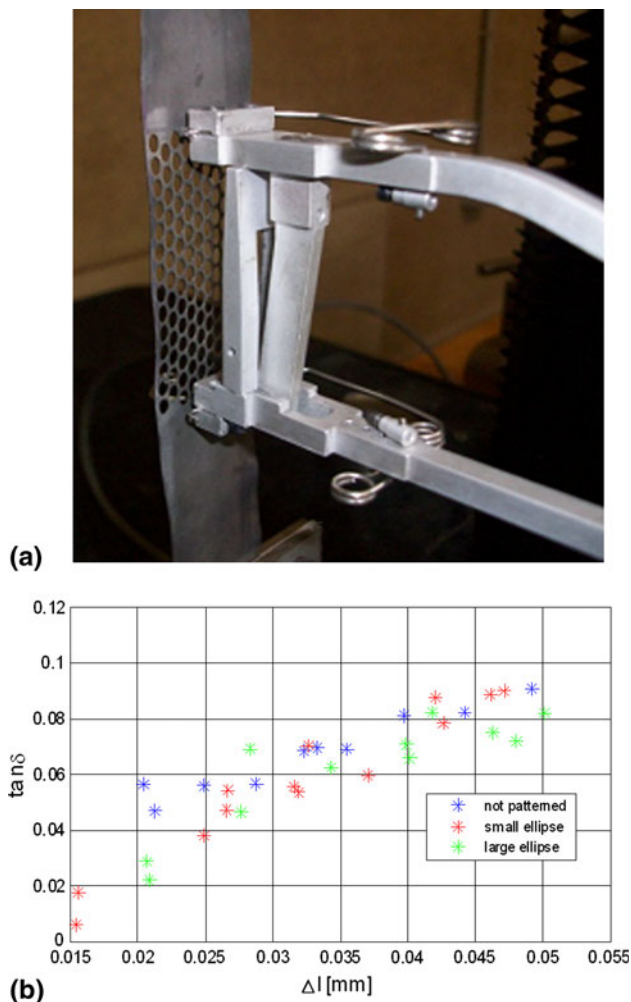
damping properties of free-standing NiTiCu ribbons. Moreover, the damping parameter tan δ increases with the applied displacement, as shown in Fig. 5(b).

The obtained damping parameter tan δ as a function of the ribbon extension Δl can be modeled with the following regressive equation (see Eq 3):

$$\tan \delta = 0.252 + 0.0552 \ln \Delta l \;(\text{mm}) \qquad \text{(Eq 3)}$$

The regressive model proposed for tan δ presents a logarithmic trend as a function of the ribbon extension. This behavior can be explained considering that in the lower range of Δl (from 0.015 to 0.042 mm) tan δ increases linearly, while for higher Δl values (exceeding 0.042 mm) tan δ is approximately constant. A logarithmic fitting therefore appears as the best way to model the measurements, being it a trend found also in several phenomena characterized by a saturation effect.

In Table 2, the main results of regression analysis are reported. The significant effect of ribbon extension Δl on tan δ and the good agreement of the proposed model with the experimental damping measurements are highlighted.

In particular, the first part of Table 2 proposes the significance of the single factors (constant factor and coefficient for ln Δl) presented in the model, characterized by a low P value (0%). The good agreement of the regressive model with the experimental data is confirmed by the adjusted coefficient of determination R^2 (adj) (73.3% in this case). When that coefficient is low, it means that the model does not express the data; on the contrary, if it is high (bigger than 60%), it means that the model gives good prediction of the experimental data. In the second part of Table 2, the low P value (0%) of the regression means that the full model is significant on the output variable (tan δ). Finally, the high P value (91.4%) of the lack of fit test points out the adequacy of the regressive model.

The damping properties of NiTiCu ribbons were also evaluated with DMA experiments in tensile configuration on thin NiTiCu stripes, in a temperature range from −20 to 120 °C. In Fig. 6, the main results of DMA testing are reported.

At temperatures above 80 °C, low tan δ and high storage modulus, typical of austenite phase, are observed. Lowering the temperature, a sudden variation of properties related to the austenite to martensite transformation can be observed at the same temperature of the DSC analysis. Moreover, lowering

Fig. 5 Tensile test configuration (a) and damping results (tan δ parameter) of NiTiCu ribbons (b)

Table 2 Table of main results of regressive analysis

Predictor	Coef	SE Coef	T	P
Constant	0.25229	0.02125	11.87	0.000
ln Δl	0.055247	0.006380	8.66	0.000
$S = 0.00737257$, $R^2 = 74.3\%$, R^2 (adj) $= 73.3\%$				

Analysis of variance

Source	DF	SS	MS	F	P
Regression	1	0.0040761	0.0040761	74.99	0.000
Residual error	26	0.0014132	0.0000544		
Lack of fit	25	0.0012530	0.0000501	0.31	0.914
Pure error	1	0.0001602	0.0001602		
Total	27	0.0054893			

the temperature below 30°C produces a second slight increase in tan δ that can be attributed to the transformation between B19 and B19′ martensites. This transformation is characterized by low enthalpy value and, especially in cold worked and low temperature heat-treated samples, can hardly be observed in calorimetric analysis.

The results in terms of damping parameter tan δ obtained with MTS system and DMA measurements are in good agreement, so they can be combined and used as input data in the following simulation on damping behavior of the laminated composite.

3.2 Characterization and Simulation of the Laminated Composite Performance

Damping properties, obtained from the described dynamic characterization of the NiTiCu ribbons, were used in conjunction with finite element method (FEM) analysis and modal strain energy (MSE) approach to calculate the laminated composite damping capacity. In the following text, the obtained results are compared with experimental results.
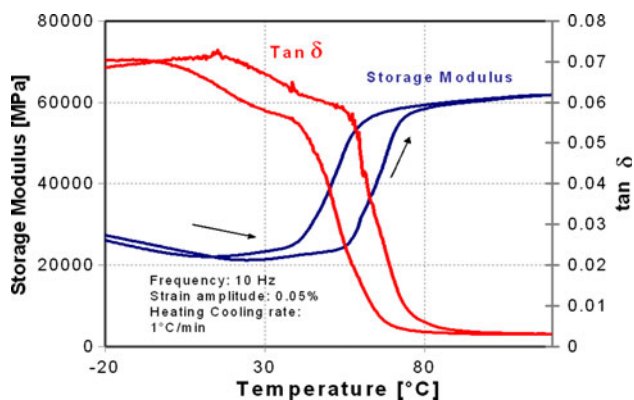

Fig. 6 DMA testing on NiTiCu ribbon

The MSE approach, used in the composite simulation performed with Abaqus 6.7, states as follow (see Eq 4):

$$\tan \delta = \sum_{i=1}^{N} \alpha_i \, \tan \delta_i, \tag{Eq 4}$$

where tan δ is the total damping of the proposed laminated composite, α_i is the elastic strain energy stored in each component, $\tan \delta_i$ is the specific damping of each component, and N indicates the number of the components (thin ribbons and matrix). The strain energy was calculated using a linear elastic, undamped, modal finite element analysis. The FE model of the laminated composite was a solid model with brick elements to simulate the GFRP core and shell elements to simulate the two patterned SMA ribbons. The constrain between upper and lower surfaces of the core and the SMA thin ribbons was a tie constrain. The numerical model of the laminated composite clamped at one end and the first flexural deformed shape is depicted in Fig. 7.

The MSE calculation was performed on an elemental basis and then summed over the entire model. The results of the FEM analysis in terms of the percentage of elastic energy stored in the SMA ribbons and in the core are summarized in Table 3. The laminated composite damping factors tan δ and h for the first flexural mode were estimated by means of Eq (4), where the average strain was equal to 0.032% and the related value of tan δ were 4 and 0.84%, respectively, for SMA ribbons and glass-fiber composite core.

It can be pointed out from the obtained results that the two different elliptical configurations do not significantly modify the first natural frequency but affect the damping behavior by modifying the energy which is stored by the SMA ribbons. Accordingly, the small ellipse configuration appears to give a better performance.

In Fig. 8(a) and (b), the estimated strain values close to the clamped end along SMA ribbon longitudinal direction are reported for the two elliptical configurations.

In order to validate the results of the simulation on the laminated composite, experimental measurements on composite damping properties were performed. The setup for the
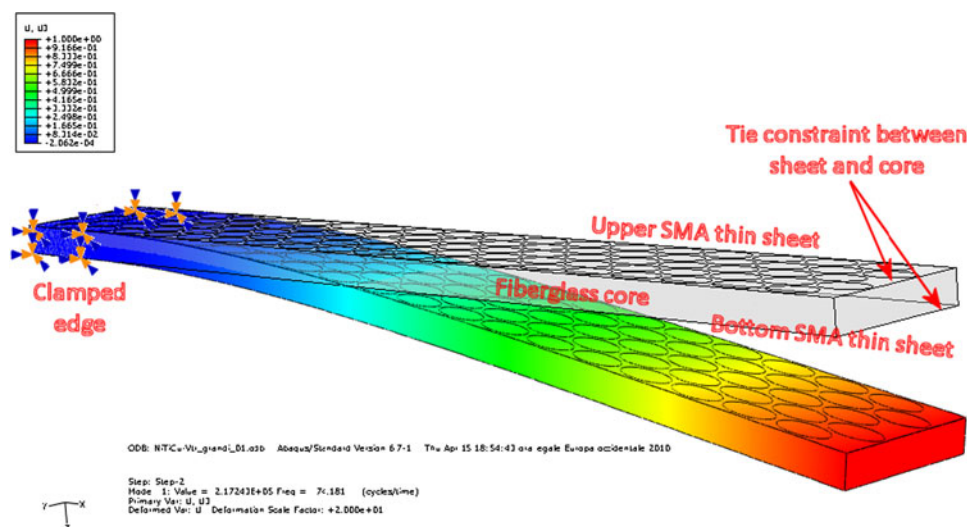

Fig. 7 Configuration of the laminated composite in the FEM simulation and the first flexural deformed shape (the displacement of the free end of the beam is set to 1). Mesh size: 0.25 mm

Table 3 Estimated damping for the first vibrational mode of the laminated composite

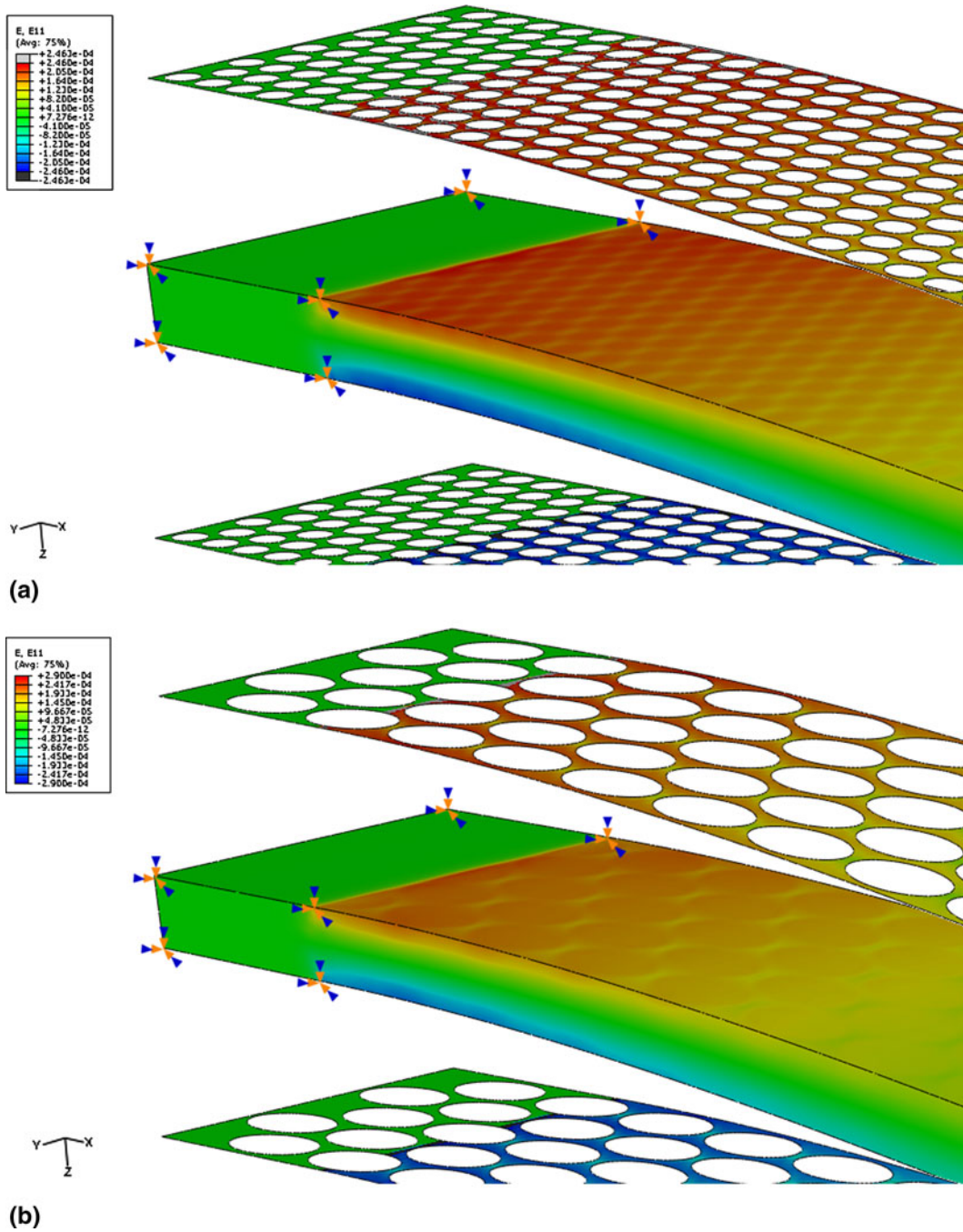| | First natural frequency, Hz | Thin ribbon elastic energy stored, % | Core elastic energy stored, % | Estimate composite damping ($\varepsilon = 0.032\%$) | |
				tan δ	h
Large ellipse	74.1	8.5	91.5	1.11	0.55
Small ellipse	74.3	10.7	89.3	1.18	0.59

Fig. 8 Calculated strains of the laminated composite with small (a) and large (b) elliptical patterned SMA ribbons

experimental measurements of the damping capacity is the same used in the simulation and shown in Fig. 7. The composite beam was clamped at one end, while an initial displacement was applied to the opposite end to start a decay transient. The decay of the vertical displacement was then measured by means of a laser triangulation transducer and the corresponding logarithmic decrement was calculated to define the damping. The decay obtained by the test on the laminated composite with small elliptical configuration SMA ribbons is reported in Fig. 9. A similar trend was obtained also in the configuration with large ellipsis. Figure 10 shows the improvement of the damping capacity in terms of h value as a function of the displacement in all the investigated configurations. When compared to glass-fiber reinforced epoxy beam (without SMA inserts), an increase of damping
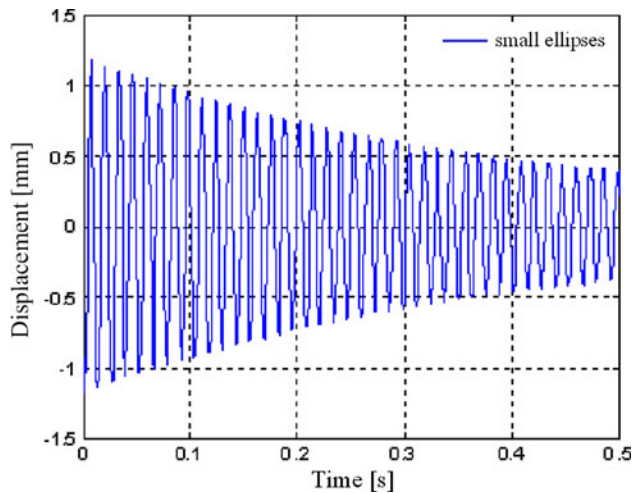
was obtained by the proposed laminated composites in the two different elliptical configurations and even with the SMA insert with no-patterned configuration. In particular, Fig. 10 shows the trend of the measured h factor as a function of the displacement for the four different laminated composites. The estimated h values for the two elliptical configurations of the laminated composite are also reported in the same figure: numerical and experimental results are in good agreement.

It can be observed that the h factor trend does not seem strongly affected by displacement, except for the laminated composite with the not patterned SMA ribbons. It is supposed that this trend could depend on the amount of SMA material introduced in the laminated composite. In fact, a bigger amount of SMA produces higher damping capacity as well a more significant effect on displacement.

Fig. 9 Experimental decay obtained on the laminated composite with small ellipses configuration of the SMA ribbons

4. Conclusions

Samples of glass-fiber composites with embedded patterned NiTiCu ribbons were produced and tested.

The behavior of the specimens was simulated with FEM analyses and MSE, using the damping properties of NiTiCu ribbon obtained from mechanical testing and DMA measurements as input data.

The experimental results were in good agreement with finite element analyses.

Improved damping properties with respect to plane glass-fiber reinforced composite were obtained and the effects of different patterns of the NiTiCu were analyzed and discussed.

In a further work, the investigations related to the identification of damping capacity of different configurations of the SMA ribbons will be improved. Besides, different types of SMAs will be investigated and the performances in terms of damping properties will be compared and discussed.
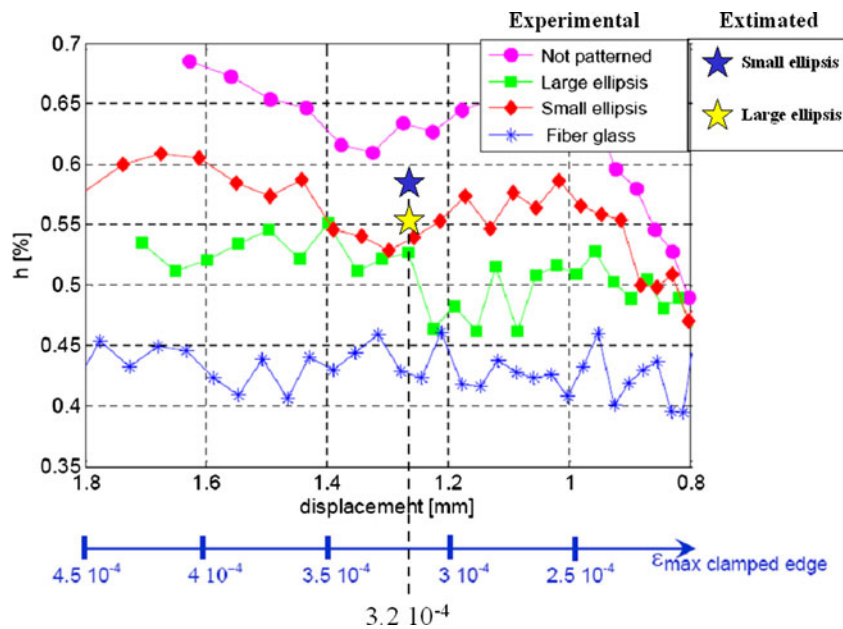

Fig. 10 Comparison between experimental and estimated damping capacity on the laminated composite

References

1. J. Van Humbeek and S. Kustov, Active and Passive Damping of Noise and Vibrations through Shape Memory Alloys: Applications and Mechanisms, *Smart Mater. Struct.*, 2005, **14**, p 171–185

2. Y. Matsuzaki, T. Ikeda, and C. Boller, New Technological Development of Passive and Active Vibration Control: Analysis and Test, *Smart Mater. Struct.*, 2005, **14**, p 343–348

3. R. Zhang, Q.Q. Ni, A. Masuda, T. Yamamura, and M. Iwamoto, Vibration Characteristics of Laminated Composite Plates With Embedded Shape Memory Alloys, *Compos. Struct.*, 2006, **74**, p 389–398

4. A. Tuissi, P. Bassani, A. Casati, M. Bocciolone, A. Collina, M. Carnevale, A. Lo Conte, and B. Previtali, Application of SMA Composites in the Collectors of the Railway Pantograph for the Italian High Speed Train, *JMEPEG*, 2009, **18**, p 612–619

5. H.C. Lin, K.M. Lin, and Y.C. Chen, A Study on the Machining of NiTi Shape Memory Alloys, *J. Mater. Process. Technol.*, 2000, **105**, p 327–332

6. C. Momma, U. Knop, and S. Nolte, Laser Cutting of Slotted Tube Coronary Stents-State of the Art and Future Developments, *Prog. Biomed. Res.*, 1999, **2**, p 39–44

7. Y.P. Kathuria, Laser Microprocessing of Metallic Stent for medical therapy, *J. Mater. Process. Technol.*, 2005, **170**, p 545–550

8. A. Schuessler, Laser Processing of Nitinol Materials, *Proceedings of SMST*, 2000, p 25–32

9. B. Previtali, S. Arnaboldi, P. Bassani, C.A. Biffi, N. Lecis, A. Tuissi, M. Carnevale, and A. LoConte, Microcutting of NiTiCu Alloy With Pulsed Fiber Laser, *ESDA2010-24943, 10th Biennial Conference on Engineering Systems Design and Analysis*, ESDA 2010, July 12-14, 2010, Istanbul, Turkey, ISBN 978-0-7918-3877-8, Order No. I844CD

10. J. Meijer, K. Du, A. Gilner, D. Hoffmann, V.S. Kovalenko, T. Masuzawa, A. Ostendorf, R. Poprawe, and W. Schulz, Laser Machining by Short and Ultrashort Pulses, State of the Art and New Opportunities in the Age of the Photons, *CIRP Ann. Manuf. Technol.*, 2002, **51**(2), p 531–550